Removal of Malachite Green from aqueous phase under ultrasound assistance using *Paracentrotus lividus* spines: equilibrium and kinetic studies

Houria Ghodbane[a],*, El Khamssa Guechi[b], Abdulaziz Alghyamah[c], Oualid Hamdaoui[c],*

[a]*Laboratory of Physics of Matter and Radiation, Department of Process Engineering, Faculty of Sciences and Technology, Mohamed Cherif Messadia – Souk Ahras University, P.O. Box: 1553, 41000 Souk Ahras, Algeria, email: hiba_ghodbane@yahoo.fr (H. Ghodbane)*
[b]*Laboratory of Environmental Engineering, Department of Process Engineering, Faculty of Engineering, Badji Mokhtar – Annaba University, P.O. Box: 12, 23000 Annaba, Algeria, email: guichi_wahida@yahoo.fr (E.K. Guechi)*
[c]*Chemical Engineering Department, College of Engineering, King Saud University, P.O. Box: 800, Riyadh 11421, Saudi Arabia, emails: ohamdaoui@ksu.edu.sa (O. Hamdaoui), aalghyamah@ksu.edu.sa (A. Alghyamah)*

Received 15 February 2020; Accepted 14 September 2020

ABSTRACT

In the present work, the *Paracentrotus lividus* spines (PLS) are proposed as a novel low-cost non-conventional adsorbent for the removal of malachite green (MG) from aqueous phases in the absence and presence of ultrasonic irradiation and by combining simultaneously ultrasound and mechanical agitation. The PLS was characterized by Fourier transform infrared spectroscopy. Batch process was used for adsorption kinetic and equilibrium studies. The effects of diverse parameters such as contact time, initial dye concentration, adsorbent dose, and solution pH on MG adsorption by PLS were investigated. The obtained results indicate that both the rate and amount of MG adsorption were enhanced in the presence of ultrasound. Dye adsorption under ultrasound assistance was improved with the increase of initial dye concentration and with decreasing the adsorbent dose. Basic pH conditions are more propitious for the adsorption of MG. The simultaneous combination of ultrasound and agitation leads to an intensification of adsorption. Adsorption isothermal data could be adequately simulated by the Langmuir model, and then Freundlich and Temkin models. Langmuir simulation indicated that the adsorption capacities of PLS spines were 22.35, 34.45, and 89.72 mg g^{-1} for the classical method, the ultrasound-assisted method, and the simultaneous association of ultrasound and stirring, respectively. The kinetic data are very well-described by the pseudo-second-order kinetics model for the classical method, ultrasound, and combining concurrently ultrasonic irradiation and stirring. The combination of ultrasound and agitation for the adsorption process has proven to be interesting for the treatment of wastewater contaminated with malachite green.

Keywords: Ultrasound; Adsorption; Malachite green; *Paracentrotus lividus* spines; Kinetics; Isotherm; Modeling

1. Introduction

Pollution induced by industrial wastewaters has become a common problem for several countries. The effluents discharged from dye manufacturing and consumption industries are very colorful coupled with high chemical and biochemical oxygen demands (COD and BOD) and having a high quantity of suspended organic solids.

Malachite green, which comes under the category of basic dyes, is widely used for coloring purposes, amongst all other dyes of its category [1]. This triarylmethane dye is largely employed in the global aquaculture industry as

* Corresponding authors.

a biocide as well as in the silk, wool, cotton, leather, paper, and in distilleries. It is also used in aquaculture as an ecto-parasiticide and a fungicide because of its efficacy and low cost. This dye can enter into the food chain and could possibly provoke carcinogenic and mutagenic effects on humans [2]. Therefore, it is crucial to remove malachite green from wastewater before rejection into the environment.

Several methods are available for treating dye impacted wastewater. Adsorption, biological oxidation, membrane separation, electrochemical techniques, and ion exchange are designated for wastewater treatment, while more attention was dedicated to adsorption. Adsorption is an inexpensive and simple process that use adsorbent to remove dye from wastewater effluent with high efficiency [3]. There is, therefore, considerable interest in developing the utilization of low-cost adsorbents for the elimination of dyes from wastewater such as agricultural wastes [4], dolomitic [5], fly ash [6], zeolite [7], chlorella [8], and sewage sludge ash [9]. The fruitful use of marine adsorbents such as sea shells [10], oyster shells [11], mussel shells [12], and scallop [13] have been reported. Since, marine adsorbents are available and can potentially be used to eliminate dye pollutants from the aqueous phase. The spines of *Paracentrotus lividus* (PLS) is selected as a suitable material for water pollutants removing.

Recently, the combination of ultrasound irradiation and the adsorption process has received a great deal of attention [14–16]. The advantage may be attached to more acceleration in chemical reactions and mass transfer as a result of acoustic cavitation (the creation, growth, and implosive collapse of bubbles in the solution) and formation of new adsorption sites on adsorbent [17–19]. The combination between ultrasound irradiation and adsorption conducts to an increase of efficiency and also a decrease of the cost of dye adsorption [16,20,21].

The purpose of this work was to investigate the potential of the spines of PLS (marine waste) as an alternative low-cost adsorbent for the removal of MG from aqueous phases in the absence and presence of ultrasound as well as by coupling ultrasonic irradiation and agitation at the same time. The effect of various experimental conditions such as contact time, initial concentration of dye, stirring speed, adsorbent dose, and ionic strength on the removal kinetics is investigated. Kinetics data are analyzed and modeled using different models. The obtained results may contribute to a better understanding of the adsorption phenomena at the liquid–solid interface in the absence and presence of ultrasound.

2. Materials and methods

2.1. Malachite green

The cationic dye (C.I. 42000; Basic Green 4), malachite green oxalate salt, (abbreviation: MG; molecular formula $C_{52}H_{56}N_4O_{12}$, FW 929), was purchased from Merck and used without further purification. The structure of this dye is displayed in Fig. 1a. Five hundred milligram per liter stock solution was prepared by dissolving the requested quantity of dye in distilled water. Working solutions at the desired concentrations were established by consecutive dilutions.

2.2. Adsorbent

The PLS were collected from the Saint Cloud sea beach in Annaba, Algeria. The spines of PLS are removed as waste. This material (PLS) was washed several times with boiled water and finally with distilled water to remove dirt particles and water-soluble materials. The washing process was continued till the wash water did not contain any color. The washed material was then completely dried in an oven at 50°C for 4 d to constant weight. The dried sample was crushed by means of a grinder into small particles of different sizes in the range of 0.5–1 mm, and stored in a desiccator for later use. No other chemical or physical treatments were used prior to adsorption experiments.

2.3. Experimental procedures

Batch adsorption experiments were performed in the experimental setup shown in Fig. 1b. Experiments were realized in a 400 mL cylindrical jacketed glass vessel that was attached to an overhead mechanical stirrer. The agitator used was a 45° pitch four blades down pumping impeller (diameter 5 cm), which has good suspension characteristics for the solid particles.

The vessel was immersed in an ultrasonic cleaning bath operating at a frequency of 45 kHz with an electrical nominal power of 120 W (indirect sonication). The ultrasonic power (69 W) was determined by the calorimetric method.

For dye removal kinetic experiments, 0.1 g of PLS was contacted with 100 mL malachite green solutions. The mixture was stirred at a fixed agitation speed of 300 rpm (classical method), sonicated, or concurrently agitated (300 rpm) and sonicated. At predetermined intervals of time, solutions were analyzed for the final concentration of malachite green by using a UV-vis spectrophotometer (Secomam, model Uviline94000) set at a wavelength of 617 nm, maximum absorbance.

All experiments were conducted in triplicate and the mean values were reported.

2.4. Material characterization

For the main functional groups that might be involved in dye adsorption, a Fourier transform infrared (SHIMADZU FTIR-8400S) analysis was done on the PLS to determine the surface functional groups, and the spectra were recorded from 4,000 to 400 cm⁻¹.

Scanning electron microscopy (SEM) pictures of PLS before and after adsorption of malachite green were taken using an environmental scanning electron microscopy (ESEM-FEI Quanta 250). The elementary composition of PLS was determined through energy-dispersive X-ray spectroscopy (EDAX TEAM EDS system) integrated with the SEM.

3. Results and discussion

3.1. Characterization of the adsorbent

3.1.1. Fourier transform infrared spectroscopy

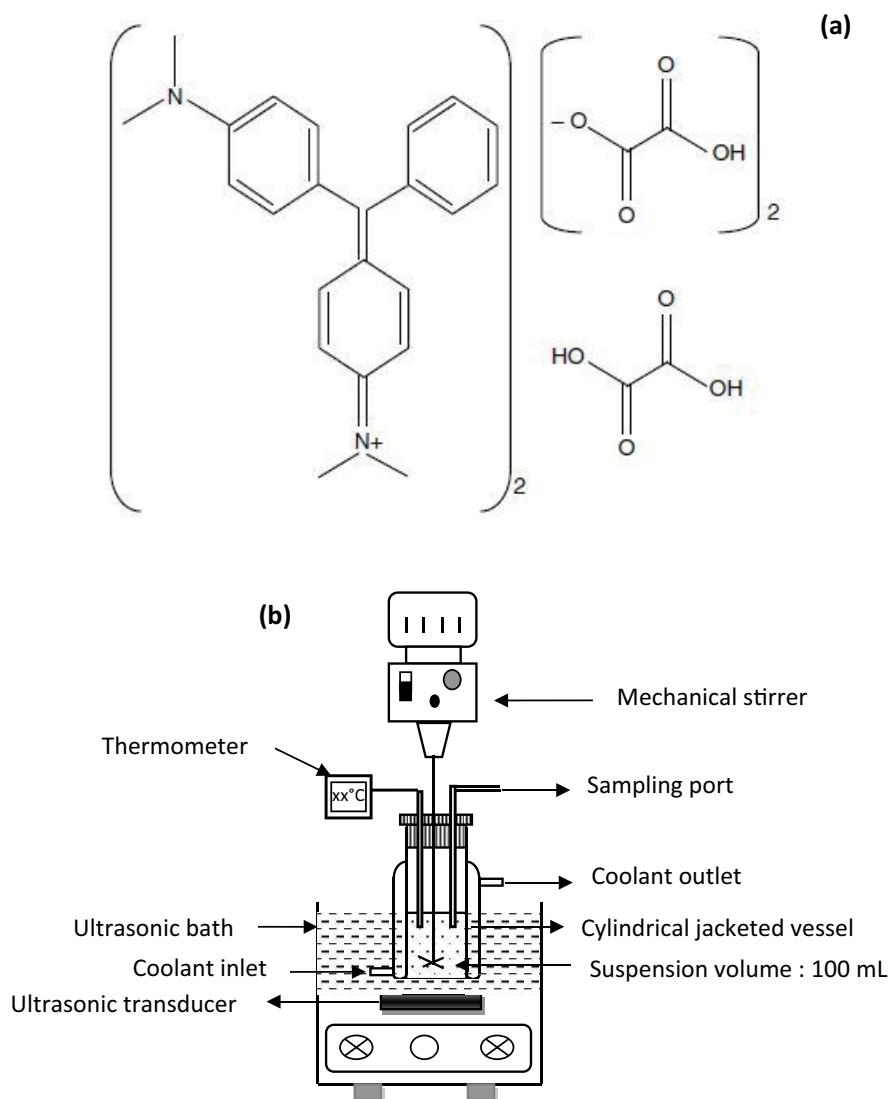FTIR spectroscopy is a widely employed method to determine the functional groups that serve as adsorption

Fig. 1. Chemical structure of malachite green (oxalate salt) (a) and experimental setup (b).

sites. FTIR spectrum for the solid waste (PLS) before and after adsorption in the absence and presence of ultrasound as well as by coupling ultrasonic irradiation and agitation is shown in Fig. 2. A clear difference was found between the adsorbent spectrum before and after adsorption. This difference largely lies in the region between 500 and 700 cm^{-1} that corresponds to the deformation vibrations due to the presence of the benzene ring, which proves the richness of the sample in aromatic compounds. The analysis of the infrared spectrum of PLS shows the following bands. It can be seen that a peak at 871 cm^{-1} represents the alkene bonds, $=CH_2$, thus the C–H of a hybridized carbon sp^2. It is the deformation vibrations. Also, we can observe a wide and intense strong band at 1,396 cm^{-1} attributed a priori to the elongation vibration of the C–H bonds of the CH_3 bonds of a sp^3 hybridized carbon, that is, alkanes and to the elongation vibrations of the C–N bond of an aromatic amine. A low-intensity peak at 2,330 cm^{-1} was appeared, which suggests that the adsorbent may contain an alkyne (C≡C)

or nitrile (C≡N) function. The elongation vibration bands that appear around 2,839 and 2,908 cm^{-1} can be attributed to the CH bonds of the alkanes. It is clearly shown that the adsorbent has a number of absorption peaks, which reflects the complex nature of the material.

An effusion due to low-intensity vibration bands in the region of 3,556 to 37,950 cm^{-1}, attributed to N–H bond elongation vibrations, was observed. This function may be due to intermolecular interactions that may form between the malachite green and the processing medium.

3.1.2. Scanning electron microscopy and X-ray dispersive energy

The SEM technique was employed to observe the surface physical morphology of the PLS (Figs. 3a–d) before and after adsorption of malachite green in the absence and presence of ultrasound and by combining concurrently ultrasonic irradiation and mechanical stirring, respectively.
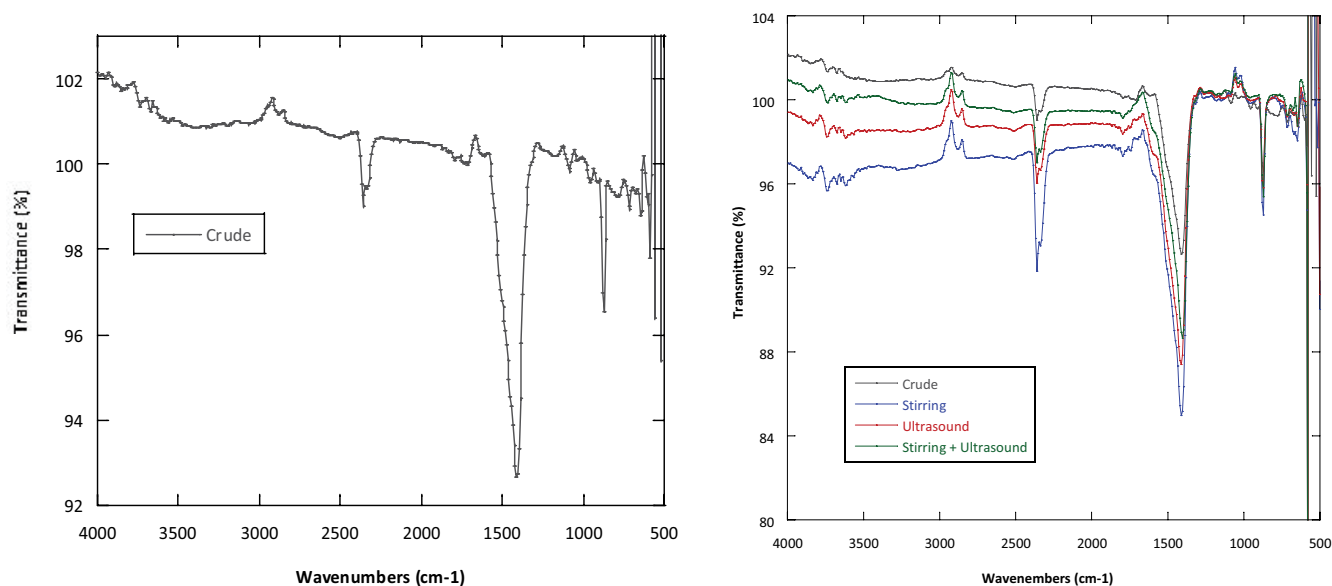
Fig. 2. FTIR spectra of PLS before and after adsorption in the absence and presence of ultrasound and in the combined process.

It is clear that PLS has a rough surface with heterogeneous pores and cavities. This indicates that there is a good possibility for MG dye to get trapped and adsorbed. The X-ray dispersive energy (EDX) analysis obtained in the spectrum presented in Fig. 3a shows the presence of Ca, O, Mg, and Al in the following proportions 24.8%, 67.6%, 5.3%, and 2.3%, respectively.

SEM characterization of PLS, before and after adsorption, showed a complete change in surface texture. Before adsorption, there was a rough surface morphology as observed, while after adsorption of dye on the PLS, layer on the surface of the adsorbent and smoother morphology was observed (Fig. 3b).

The surface became rough with a new porous structure created in the presence of ultrasound as shown in Figs. 3c and d. The formation of the porous structure is due to the hydrodynamic cavitation effect of ultrasound. It enhances the adsorption efficiency of the adsorbent through the active site created, which provides a larger surface area for the dye molecules to attach with.

3.2. Effects of ultrasound and contact time

Fig. 4 shows the results of MG adsorption kinetics by PLS in the absence (classical method by simple mechanical agitation) and the presence of ultrasound (40 kHz and 69 W) as well as in the combined process (ultrasonic irradiation and mechanical agitation simultaneously). The rate and amount of adsorption were significantly increased and enhanced in the presence of ultrasound.

Sonication improved the removal of MG through the extreme conditions produced by cavitation bubbles. The improvement in adsorption may be caused by an alteration in the equilibrium and enhancement of adsorption kinetics. Additionally, ultrasound can increase the rate of adsorption by expediting mass transfer by hydrodynamical effects produced by acoustic cavitation [22–25].

Microjets and shockwaves generated by the cavitation may change the structure of the adsorbent and lead to a higher adsorption capacity. A further improvement of the dye removal is assigned to thermal properties induced by localized hot spots formed when bubbles cavitated [23–25].

As it is illustrated in Fig. 4, the dye adsorption in the presence of ultrasound alone and in the combined process (sonication and mechanical mixing) reached equilibrium in about 130 min, but in the classical method, this time is expanded to about 600 min. The rate of removal of MG and the adsorption capacity of the adsorbent in the combined method were higher than those obtained by simple agitation and by ultrasound alone. The shorter time to achieve equilibrium and the faster rate of removal in the combined process was assigned to the strong convective currents occurring within the reactor. These effects associated with the hydrodynamic phenomena caused by cavitation and mechanical agitation are responsible for the perfect mixing of the reactor content.

3.3. Effect of initial dye concentration

The effect of MG initial concentration on the dye adsorption by PLS for the conventional method, sonication, and combined method is illustrated in Fig. 5. The obtained results displayed that the dye removal varied with changing initial MG concentration. The adsorption efficiency of MG increased progressively with increasing contact time and achieved a plateau thereafter. An increase in initial dye concentration leads to an increase in the adsorption capacity of PLS, especially in the presence of ultrasound (Fig. 5). When initial dye concentration was increased from 5 to 15 mg L^{-1}, after 130 min of treatment, the adsorption capacity increased, respectively, from 2.78 to 6.41 mg g^{-1} by the conventional method, from 4.66 to 14.09 mg g^{-1} by sonication alone, and from 5 to 14.1 mg g^{-1} by combining ultrasonication and mechanical stirring. For all initial
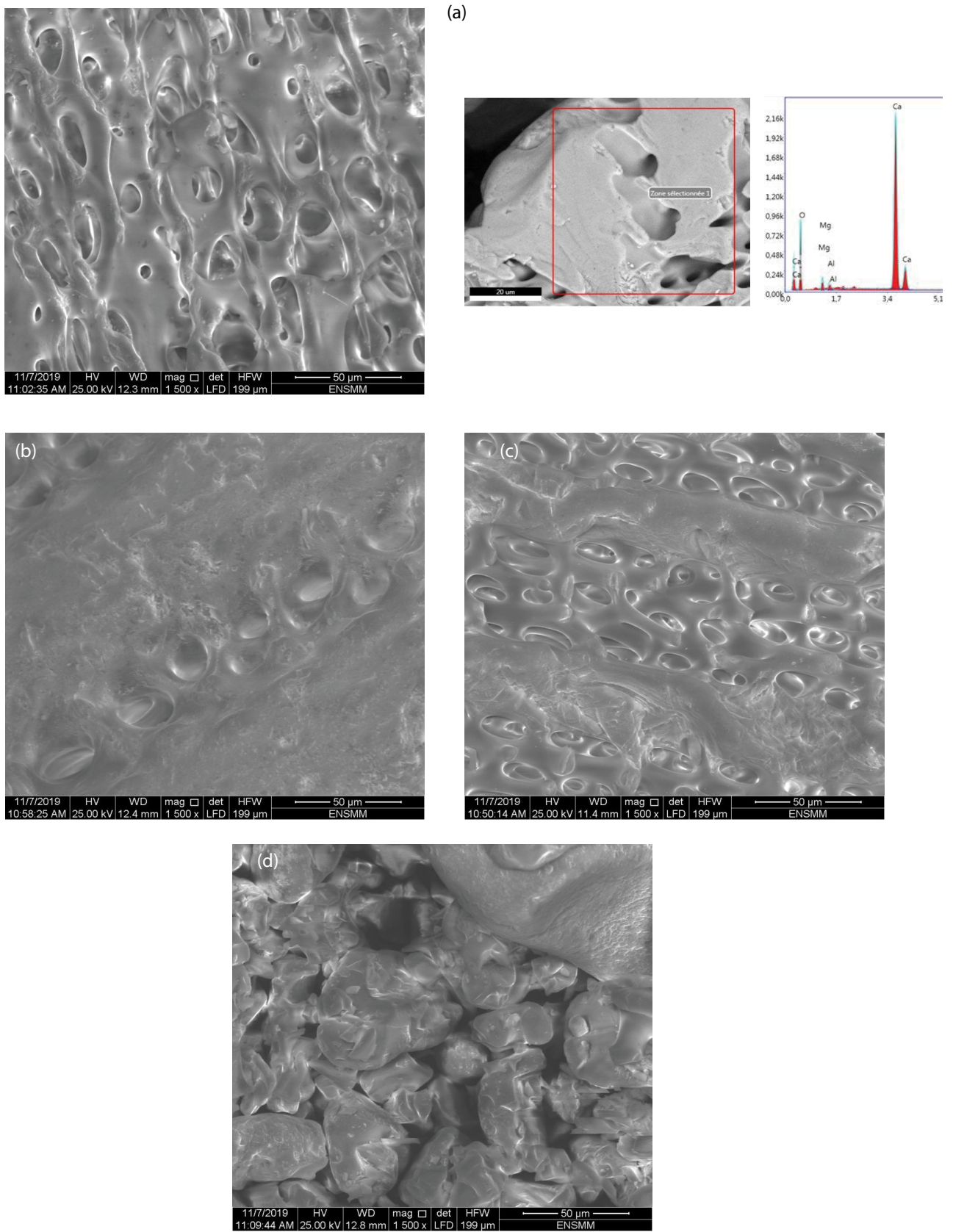
Fig. 3. (a) SEM images and EDX spectrum of PLS. SEM image of adsorbent after adsorption by (b) conventional method, (c) sonication without stirring, and (d) combined method.
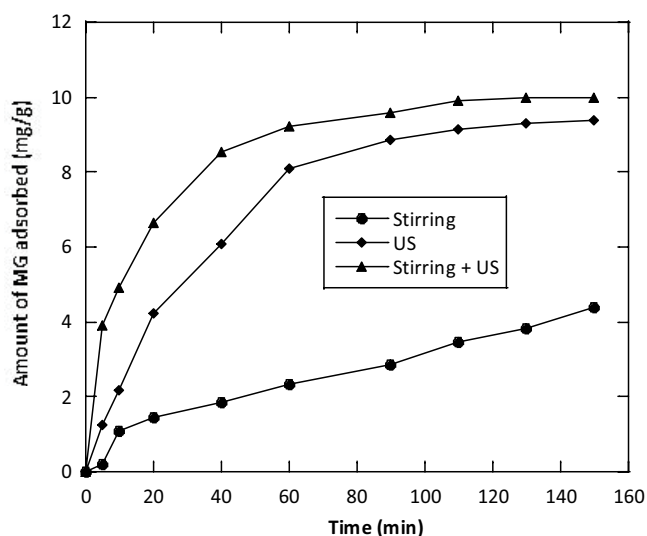
Fig. 4. Adsorption of malachite green by PLS in the absence and presence of ultrasound and in the combined process ($T = 21°C$, adsorbent dose = 0.1 g/100 mL, initial dye concentration = 10 mg L^{-1}, and acoustic power = 69 W).
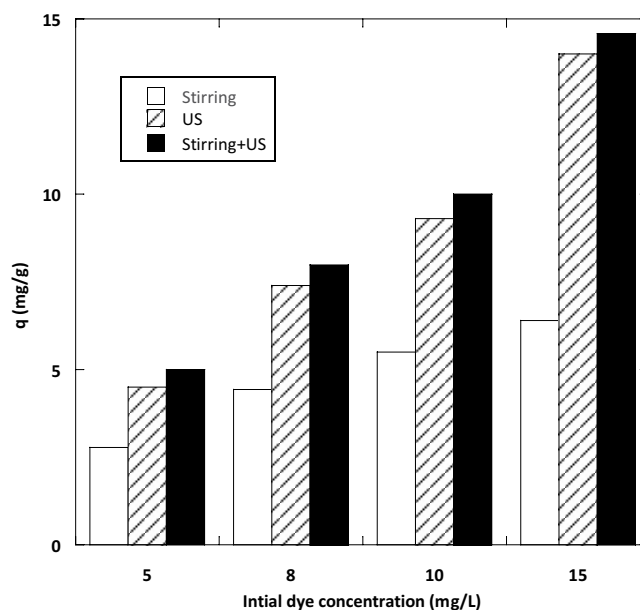

Fig. 5. Amount of malachite green adsorbed at equilibrium in the absence and presence of ultrasound and in the combined method for different initial dye concentrations ($T = 21°C$, adsorbent dose = 0.1 g/100 mL, initial dye concentration = 5–15 mg L^{-1}, and acoustic power = 69 W).

dye concentrations, higher adsorption occurred using the combination of ultrasonic irradiation and mechanical stirring than with the classical method. The enhancement of adsorption by sonication can be explained by the intensification of mass transfer phenomena and the thermal effects of ultrasound. By the combination of sonication and mechanical agitation, the perfection of the MG removal is due to the perfect mixing produced in the reactor. This behavior could be attributed to the induction of turbulence and additional convective mass transport within the pores and at the surface induced by high-speed microjets and high-pressure shock waves and also by microstreaming.

3.4. Effect of adsorbent dosage

To examine the effect of adsorbent dose on MG adsorption, experiments were conducted at an initial dye concentration of 10 mg L^{-1}. The effect of adsorbent dose on the amount of MG adsorbed for the conventional method, sonication, and for the combined method (ultrasound + stirring) is shown in Fig. 6a. In all cases, it was observed that the amount of MG adsorbed decreased with the increase in adsorbent dose. After 130 min of treatment, the adsorbed amount decreased from 5.5 to 1 mg g^{-1} for the conventional method, from 9.14 to 1.21 mg g^{-1} for ultrasound-assisted method, and from 10 to 1.25 mg g^{-1} for the combined method for an increase in adsorbent dose from 0.1 to 0.8 g/100 mL, respectively.

The diminution in the amount of MG adsorbed with increasing adsorbent mass is attributable to the split in the flux or the concentration gradient between solute concentrations in the solution and on the adsorbent surface. But dye removal increases with an increase in the adsorbent dose. The increase in MG removal was attributable to the increase of the available adsorption surface and the availability of more adsorption sites. Hence, with increasing adsorbent mass, the amount of dye adsorbed by the unit

weight of adsorbent diminished, thus causing a decrease in adsorption capacity with increasing adsorbent dosage. For all adsorbent dosages, it was indicated that adsorption was more effective in the presence than in the absence of ultrasound. Additionally, the elimination of dye increased in the presence of ultrasound more than with the classical method. This could be related to the higher mass transfer in the presence of the ultrasonic irradiation. For the highest adsorbent dose, the increase of adsorption in the presence of ultrasound is low, which is explained by the high availability of adsorption sites (Fig. 6a).

The amount of MG adsorbed in the presence of the ultrasonic field is higher than that obtained in the conventional method, whatever the adsorbent dose is. This behavior could be related to the physical effects of ultrasound and cavitation, which give rise to strong convection in the medium through various physical phenomena. Adsorption, being a mass transfer process, is limited by diffusion–convection in the system. The overall resistance to mass transfer can be reduced by increasing the convection in the medium or, in other words, making the system turbulent. When the bubble is collapsing near the solid surface, symmetric cavitation is hindered and collapse occurs asymmetrically. The asymmetric collapse of bubbles in a heterogeneous system produces high-speed microjets. Additionally, symmetric and asymmetric collapses generate shockwaves, which cause extremely turbulent flow at the liquid–solid interface, increasing the rate of mass transfer near the solid surface. Furthermore, the cavitation event also gives rise to acoustic microstreaming or formation of miniature eddies that enhance the mass and heat transfer at interfacial films surrounding nearby sorbent particles and within the pores. As a result, sonication could produce not only high-speed microjets but also
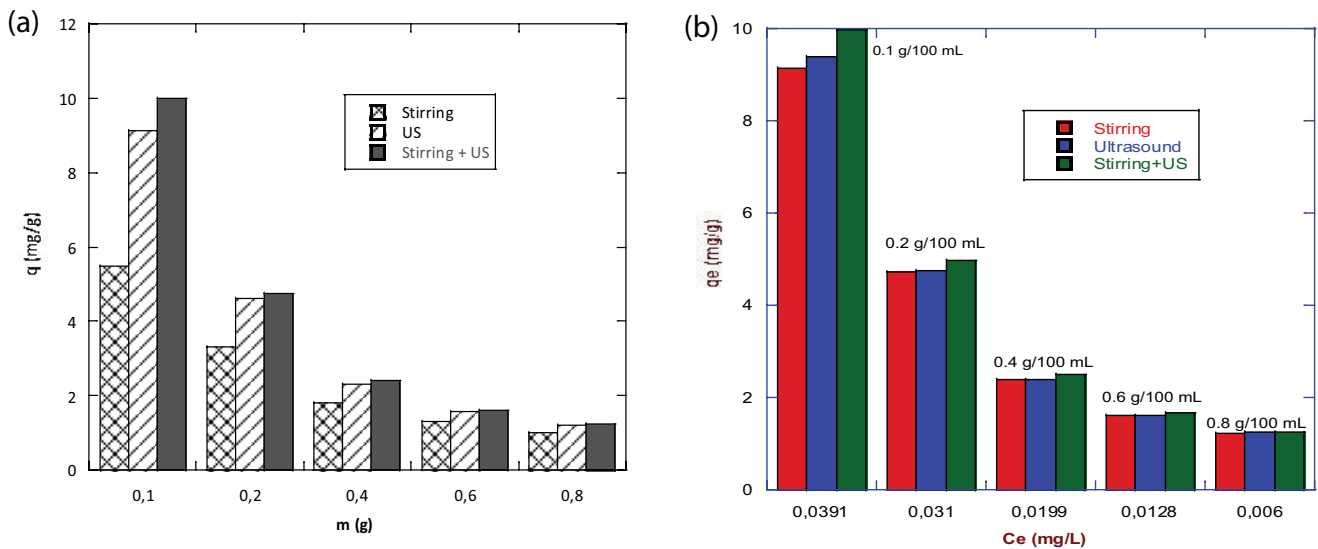
Fig. 6. (a) Amount of malachite green adsorbed at equilibrium in the absence and presence of ultrasound and in the combined method for different adsorbent dosages and (b) adsorbed amount of dye at equilibrium as function of the equilibrium concentration of malachite green in liquid phase for the three tested methods (T = 22°C, adsorbent dose = 0.1–0.8 g/100 mL, initial dye concentration = 10 mg L^{-1}, and acoustic power = 69 W).

high-pressure shock waves and acoustic vortex microstreaming [24–31]. These actions lead to an improvement of the adsorption by an enhancement of mass transfer. On the other hand, t the movement of cavitation bubbles in liquid causes a flow of the liquid termed acoustic streaming or microstreamer, which increases the mass transfer.

For an adsorbent dose of 0.8 g/100 mL, the adsorption capacity increased from 1.00 mg g^{-1} in the conventional method to 1.2 mg g^{-1} in presence of ultrasound and 1.25 mg g^{-1} in the combined process.

For various adsorbent dose ranging from 0.1 to 0.8 g/100 mL, the amount of MG adsorbed at equilibrium as function of the equilibrium concentration of dye for the conventional method, for the assistance of ultrasound, and for the simultaneous association of ultrasound and stirring (combined method) is shown in Fig. 6b.

3.5. Effect of solution pH

The pH is an important parameter to be taken in consideration for the removal of dyes from aqueous phases, as it can affect the interaction between adsorbent and adsorbate, and also it can affect the charge at the surface of the adsorbent [32]. pH$_{pzc}$ of PLS is equal to 8.9. The effect of pH solution on the amount of MG adsorbed for the conventional method, for the assistance of ultrasound, and for the simultaneous association of ultrasound and stirring (combined method) is shown in Fig. 7. The results presented in Fig. 7 show that the effect of pH is almost insignificant on the adsorption capacity. During the pH effect experiments, the final pH of suspensions with initial pH values of 4–8 converged rapidly (<5 min) to pH$_{PZC}$ (8.9). At initial pH < pH$_{PZC}$, H$^+$ ions may be exhausted by reducing functional groups on the adsorbent surface, while at higher pH values, the released H$^+$ of hydroxyl and/or carboxyl groups may neutralize the alkali solution [37].

3.6. Isotherm analysis

The adsorption isotherm is essentially important for describing how the solutes interact with the adsorbents and is fundamental to optimize the utilization of the adsorbents. In order to determine the most suitable correlations for the equilibrium data in the adsorption design system, three currently used isotherm models were tested: the Langmuir, the Freundlich, and the Temkin models.

The applicability of the isotherm equations was compared by evaluating the correlation coefficients, R. The Langmuir [33] adsorption model has predicated on the hypothesis that maximum adsorption corresponds to a saturated monolayer of solute on the adsorbent surface. This model suggests that all adsorption sites are supposed to be identical. Each site holds one molecule of the given compound and all sites are energetically and sterically independent of the adsorbed amount. The linear form of the Langmuir equation can be depicted by:

$$\frac{C_e}{q_e} = \frac{1}{q_m}C_e + \frac{1}{b \cdot q_m} \tag{1}$$

where C_e (mg L^{-1}) is the equilibrium concentration of the dye, q_e (mg g^{-1}) is the amount of adsorbate per unit mass of adsorbent, q_m (mg g^{-1}), and b (L mg^{-1}) are Langmuir constants related to adsorption capacity and rate of adsorption, respectively.

The linear plot of specific adsorption (C_e/q_e) against the equilibrium concentration (C_e) is depicted in Fig. 8. This figure shows that the adsorption obeys the Langmuir model. The Langmuir constants q_m and b were determined from the slope and intercept of the plot and are presented in Table 1. The correlation coefficient values indicate that the Langmuir isotherm offers a good adjustment to the isotherm data for the three investigated methods. The principal characteristics
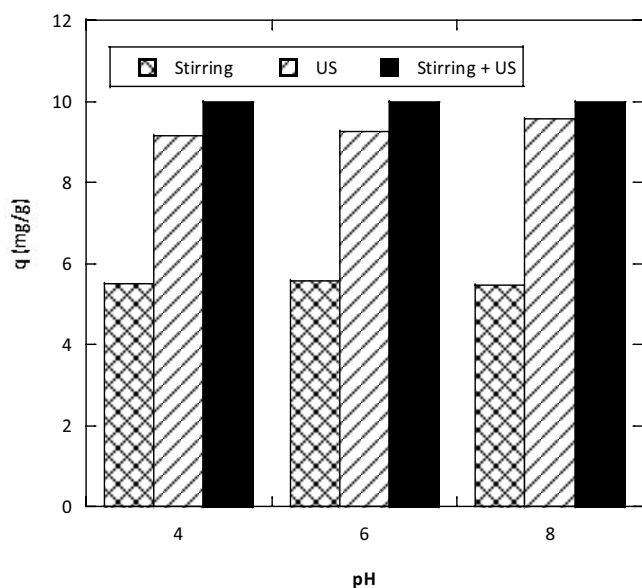
Fig. 7. Amount of malachite green adsorbed at equilibrium in the absence and presence of ultrasound and in the combined method for different pH (T = 21°C, pH = 4–8, initial concentration = 10 mg L^{-1}, adsorbent dose = 0.1 g/100 mL, and sonication power = 69 W).

of the Langmuir isotherm maybe outlined in terms of the constant dimensionless separation factor R_L [34] given by Eq. (2).

$$R_L = \frac{1}{1 + bC_0} \tag{2}$$

where C_0 (mg L^{-1}) is the initial dye concentration and b (L mg^{-1}) is the Langmuir constant. The parameter R_L (Fig. 9) specifies the nature of the type of form of the isotherm to be either unfavorable ($R_L > 1$), linear ($R_L = 1$), favorable ($0 < R_L < 1$), or irreversible ($R_L = 0$). For the adsorption of MG by PLS, the values of R_L are in the range of 0.08536–0.1548 for the three investigated methods, which demonstrate that the uptake of MG is a favorable process.

The equilibrium data were analyzed by linear regression analysis method to fit the Freundlich model. The linear form of the Freundlich model is represented by Eq. (3):

$$\ln q_e = \ln k_F + \frac{1}{n} \ln C_e \tag{3}$$

where q_e (mg g^{-1}) is the amount adsorbed at equilibrium, C_e (mg L^{-1}) is the liquid-phase concentration at equilibrium, k_F (mg$^{1-(1/n)}$ L$^{1/n}$ g^{-1}) is the Freundlich constant that is used as an indicator of adsorption capacity, and n is a constant depending to the magnitude of the adsorption driving force. A linear plot of $\ln q_e$ against $\ln C_e$ was employed to give the values of k_F and n from the slope and intercept of the line (Fig. 10). The Freundlich parameters are recapitulated in Table 1. The correlation coefficients (R) showed relatively good linearity. The Freundlich adsorption capacity parameters k_F for the removal of MG by adsorption on PLS obtained in the combined method and in the presence of ultrasound
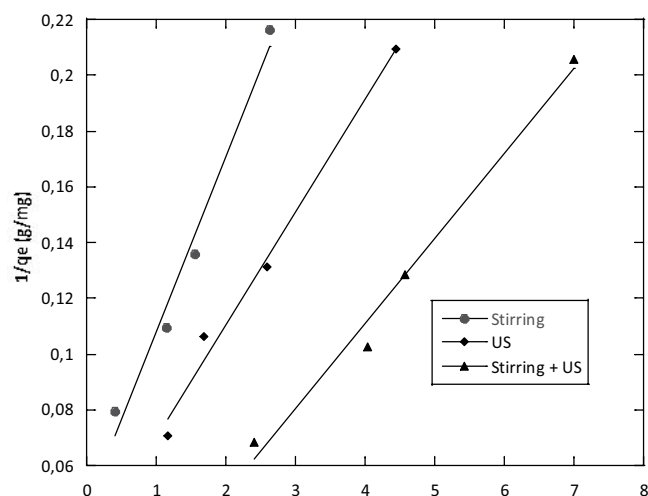

Fig. 8. Langmuir adsorption isotherm for MG by PLS (conditions: 100 mL of MG solution, initial concentrations: 5–15 mg L^{-1}, adsorbent mass: 0.1 g, acoustic power: 69 W, stirring speed: 300 rpm, pH 4, and temperature: 25°C).
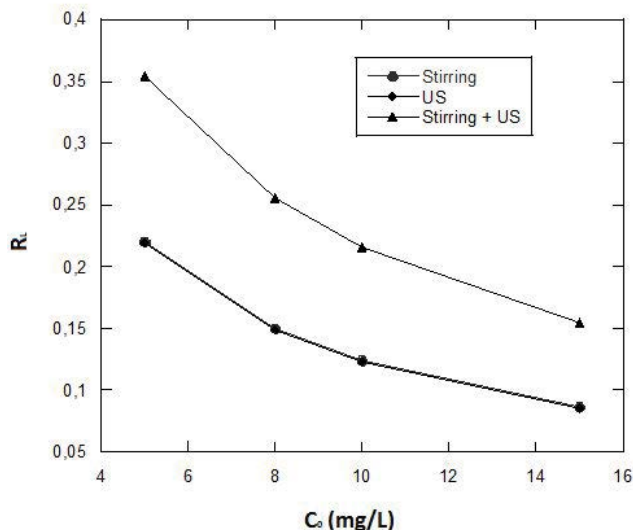

Fig. 9. Evolution of the Hall parameter, calculated from the equation of Langmuir, depending on the initial concentration.

are higher compared to that resulting from the conventional method. This is an indication that under sonication, new adsorption sites occurred by disturbance of the adsorbent particles.

The Temkin isotherm [35] is focused on the assumption that the heat of adsorption would reduce linearly with increasing adsorbent coverage. The linear form of the Temkin equation can be depicted by:

$$q_e = \frac{R_g T}{b_t} \ln a_t + \frac{R_g T}{b_t} \ln C_e \tag{4}$$

where b_t is the Temkin constant related to the heat of adsorption (J mol^{-1}), a_t is the Temkin isotherm constant
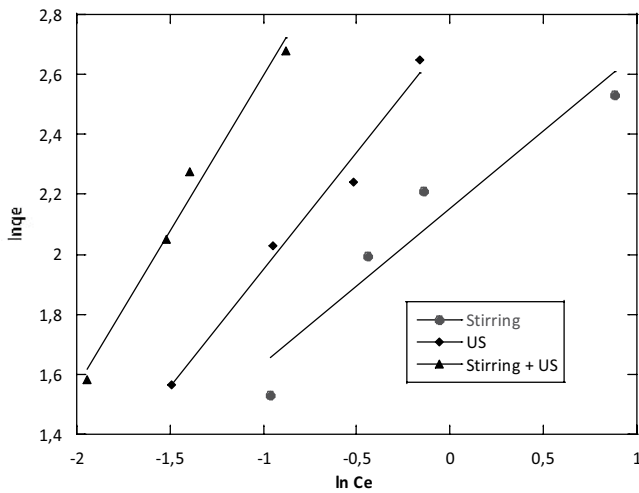
Fig. 10. Freundlich adsorption isotherm for MG adsorption by PLS (conditions: 100 mL of MG solution, initial concentration: 5–15 mg L^{-1}, adsorbent mass: 0.1 g, acoustic power: 69 W, stirring speed: 300 rpm, pH 4, and temperature: 21°C).

(L mg^{-1}), R_g is the ideal gas constant (8.314 J mol^{-1} K^{-1}), and T is the absolute temperature (K).

The adsorption data for MG by PLS were analyzed by a linear regression analysis to fit the Temkin isotherm model (Fig. 11). The parameters of Temkin model as well as the correlation coefficients are listed in Table 1. The coefficients of correlation were high representing good linearity. It was noted that the Temkin constant, a_t, increases with a considerable improvement in the combined method, whereas the Temkin constant, b_t, due to the heat of adsorption reduced under the assistance of ultrasound. The Temkin constant related to the heat of adsorption was found to be small in all cases with the order: combined method (264.79 J mol^{-1}) < sonication alone (370.52 J mol^{-1}) < conventional method (578.27 J mol^{-1}). However, the typical range of bonding energy for the ion exchange mechanism is 8–16 kJ mol^{-1} [36]. As the binding energy range related to the adsorbent under study was found to be substantially low, the interaction between the adsorbate and the adsorbent appeared to be lower, according to the degree of their obeisance to Temkin's model (i.e., the degree of linearity of the heat of adsorption).

Table 2 lists a comparison of the adsorption capacity of the PLS with those obtained in the literature for the adsorption of MG. The calculated adsorption capacities exhibit a good capacity for dye adsorption from aqueous solutions. This result reveals that the PLS is an effective adsorbent for MG dye removal from wastewater when it was used in the combined method. It should be noted that the values and comparisons reported for MG dye removal capacity have only a relative meaning because of different testing conditions and methods.

3.7. Modeling of adsorption kinetics

A simple kinetic model was employed to test the experimental data obtained via the three methods investigated for different initial concentrations by using the equation of Lagergren [55], which is the first elaborated

Table 1
Isotherm parameters for the adsorption of MG by PLS

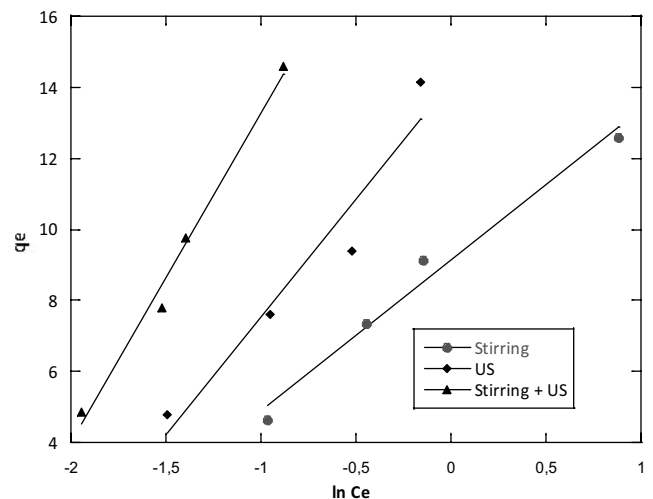|	Stirring	Sonication	Combined method
Langmuir			
b (L mg^{-1})	0.7097	0.7149	0.3656
q_m (mg g^{-1})	22.3513	34.4483	89.7182
R	0.9881	0.9938	0.9934
Freundlich			
n	1.9346	1.2807	0.9648
K_F (mg$^{1-(1/n)}$ L$^{1/n}$ g^{-1})	8.6166	15.3451	37.9511
R	0.9572	0.9910	0.9914
Temkin			
a_t (L mg^{-1})	8.6072	8.4850	11.4112
b_t (J mol^{-1})	578.2731	370.5158	264.7942
R	0.9901	0.9653	0.9938

Fig. 11. Temkin adsorption isotherm for MG adsorption by PLS (conditions: 100 mL of MG solution, initial concentration: 5–15 mg L^{-1}, adsorbent mass: 0.1 g, acoustic power: 69 W, stirring speed: 300 rpm, pH 4, and temperature: 21°C).

equation that can be used to describe the adsorption of liquid–solid systems based on solid capacity.

$$\ln(q_e - q) = \ln q_e - k_1 t \qquad (5)$$

where q_e (mg g^{-1}) is the amount of MG adsorbed at equilibrium, q (mg g^{-1}) is the amount of MG adsorbed at time t and k_1 (min^{-1}) is the rate constant of pseudo-first-order adsorption. A linear plot of $\ln(q_e - q)$ against time allows obtaining the rate constant (Fig. 12). If the plot was found to be linear with a good correlation coefficient, it indicates that Lagergren's equation is appropriate to MG adsorption by PLS. The Lagergren's pseudo-first-order rate constant (k_1) and q_e determined from the model are depicted in Table 3, along with the corresponding correlation coefficients. It was

Table 2
Comparison of adsorption capacity of the PLS with that of various adsorbents

Adsorbent	q_m (mg g^{-1})	Reference
Bentonite clay	7.716	[37]
Arundo donax root	8.490	[38]
Rattan sawdust	62.7 ± 1.27	[39]
Dead pine needles	33.56	[26]
Neem sawdust	4.35	[40]
Degreased coffee bean	55.3	[41]
Pine wood decayed by fungi *Poria cocos*	16.093	[42]
Limonia acidissima (wood apple) shell	35.84	[43]
Sea shell powder	42.3	[10]
Avena sativa (oat) hull	51.42	[44]
Cerastoderma lamarcki shell	35.84	[45]
Zeolite	19.70	[46]
Iron humate	19.2	[47]
Composite of coir pith activated carbon (CPAC)	4.4	[48]
CPAC/chitosan/SDS	4.8	[48]
Leaves of *Solanum tuberosum*	33.3	[49]
Carbon prepared from Borassus bark	20.70	[50]
Dried cashew nut bark carbon	20.09	[51]
Chlorella-based biomass	18.4	[8]
Cellulose powder	2.422	[52]
Rice husk	7.40	[53]
Tamarind fruit shell	1.95	[54]
PLS (Conventional method)	22.351	This work
PLS (Ultrasound-assisted method)	34.448	This work
PLS (Combined method)	89.718	This work

observed that for the three methods, the correlation coefficients are acceptable ($R \geq 0.9614$). Also, it was found that the values of the adsorption capacity at equilibrium determined theoretically are not close compared to the experimental values, especially for the case of combined method and ultrasound alone, which shows that the Lagergren model is not suitable for describing the adsorption of the dye by the biomaterial.

The adsorption kinetics can also be described by the pseudo-second-order equation [56,57]:

$$\frac{t}{q} = \frac{1}{K_2 q_e^2} + \frac{1}{q_e} t \tag{6}$$

where k_2 (g mg^{-1} min^{-1}) is the pseudo-second-order rate constant. The q_e and k_2 values can be determined from the slope and intercept of the plot t/q vs. t (Fig. 13). The pseudo-second-order rate constants k_2 and the corresponding linear regression correlation coefficients are given in Table 3. The correlation coefficient values were found to be in the range of 0.9731–0.9999. Moreover, the variations between the calculated q_e and experimental q_e were very minimal for this model, especially in the case of the combined method. Therefore, it can be concluded that the pseudo-second-order

kinetics model provided a better correlation for the adsorption of MG by PLS at different initial dye concentrations compared to the pseudo-first-order model for the three methods. Hubbe et al. [58] mentioned that a majority of studies that have shown good fits to the pseudo-second-order (PSO) model have involved relatively small and simple adsorbate species. Since small molecules and ions tend to diffuse rapidly in solution, they would be able to adopt essentially all of their possible molecular conformations within tiny pore spaces in fractions of seconds, including high numbers of collisions with, and possible detachments from, an adjacent solid surface.

The fact that data more often fit better to a PSO rate expression implies that the rate of uptake slows down to a greater extent than one would expect based on the mere filing of adsorption sites. Of the several contributing explanations, one of the most persuasive involves the selection of experimental conditions [58].

Hubbe et al. [58] reported also that there are two main strategies that researchers have used in published works to provide an explanation for good fits of adsorption data to pseudo-second-order kinetics. The first of these sets of strategies are mathematical or statistical, arguing that the good fits are merely a consequence of how random errors can be expected to affect the analysis of data. Such an approach can
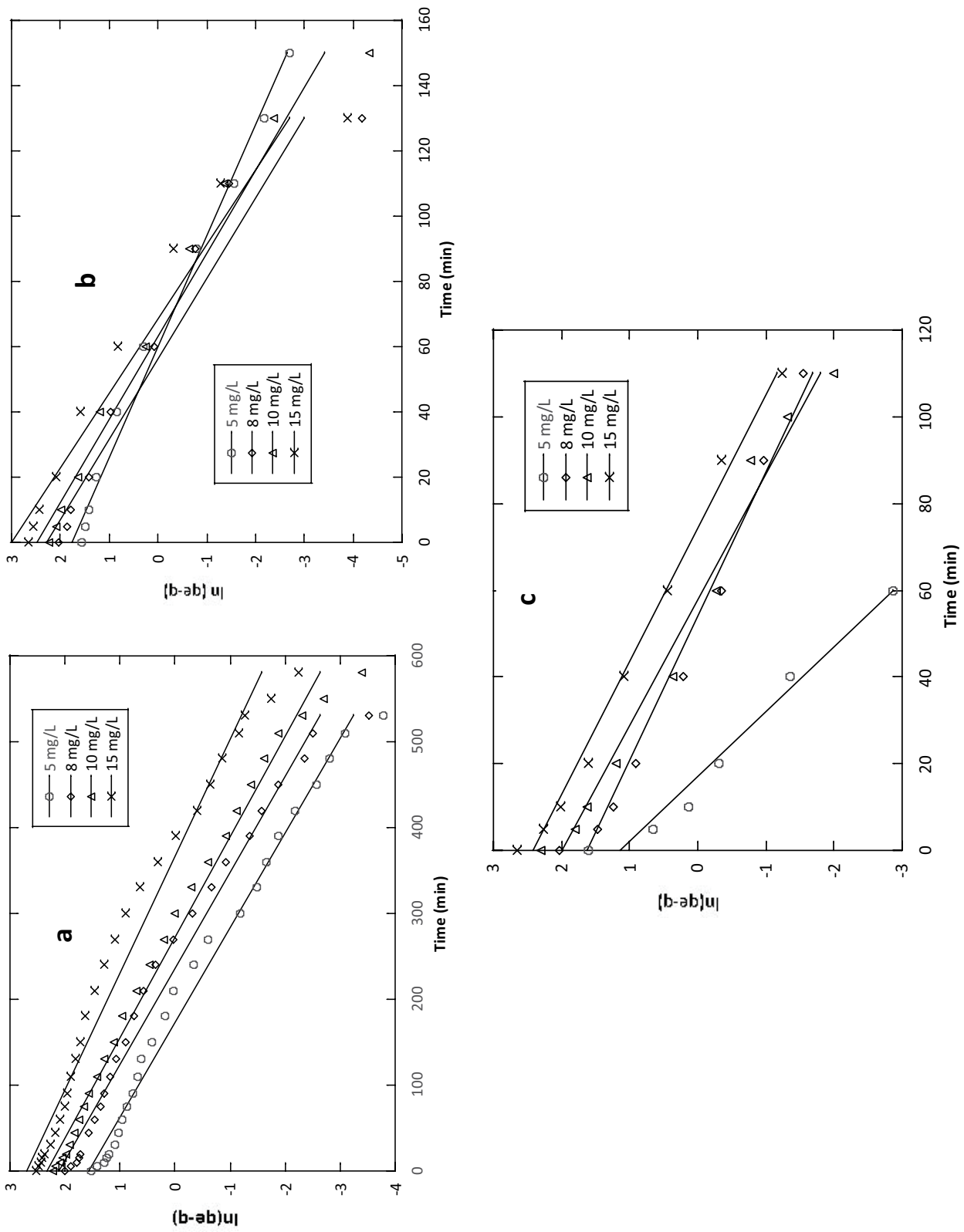
Fig. 12. Pseudo-first-order kinetics for the adsorption of MG by PLS: (a) conventional method, (b) sonication, and (c) combined method (conditions: 100 mL of MG solution, initial concentration: 5–15 mg L^{-1}, adsorbent mass: 0.1 g, acoustic power: 69 W, stirring speed: 300 rpm, pH 4, and temperature: 21°C).

Table 3
Comparison of the pseudo-first-order and pseudo-second-order parameters for the adsorption of Malachite Green at various initial concentrations (conditions: 100 mL of MG solution, initial concentration: 5–15 mg L^{-1}, adsorbent mass: 0.1 g, acoustic power: 69 W, stirring speed: 300 rpm, and temperature: 21°C)

C_0 (mg L^{-1})	$q_{e,exp}$ (mg g^{-1})	Pseudo-first-order model			Pseudo-second-order model		
		k_1 (min^{-1})	$q_{e,calc}$ (mg g^{-1})	R	k_2 (g mg^{-1} min^{-1})	$q_{e,calc}$ (mg g^{-1})	R
Conventional method							
5	4.6189	0.0090	4.8172	0.9928	0.0022	5.3222	0.9947
8	7.3585	0.0089	8.2523	0.9862	0.0012	8.6296	0.9944
10	9.1333	0.0085	10.1868	0.9917	0.0007	11.1943	0.9972
15	12.5783	0.0073	14.7037	0.9845	0.0003	16.0751	0.9950
Ultrasound-assisted method							
5	4.7751	0.0294	5.8949	0.9947	0.0012	8.1287	0.9731
8	7.6138	0.0405	9.8552	0.9614	0.0029	9.5383	0.9952
10	9.4047	0.0393	12.0661	0.9826	0.0024	11.6195	0.9959
15	14.1488	0.0439	20.1963	0.9655	0.0011	18.6008	0.9887
Combined method							
5	5.0000	0.0668	3.1515	0.9836	0.0509	5.2145	0.9999
8	7.6509	0.0301	5.1279	0.9867	0.0126	8.1300	0.9995
10	9.9739	0.0345	7.3713	0.9896	0.0085	10.7808	0.9997
15	14.1030	0.0326	11.3169	0.9953	0.0046	15.5077	0.9997

be used, for instance, to assert that apparent fits to a PSO model are actually attributable to an underlying pseudo-first-order (PFO) mechanism.

Therefore, the kinetics data were further evaluated by the intraparticle diffusion model to elucidate the diffusion mechanism, which is defined as follows [59]:

$$q = k_i t^{1/2} + C_i \tag{7}$$

where q is the amount of MG adsorbed (mg g^{-1}) at time t, k_i is the intraparticle diffusion constant (mg g^{-1} min$^{-1/2}$), and C_i is the intercept.

Fig. 14 shows the amount of MG adsorbed vs. $t^{1/2}$ for intra-particle diffusion at different initial dye concentrations for the conventional method, sonication alone, and the combined method. The obtained results showed that the curves have three successive linearities: the first is instantaneous adsorption on the external surface of the solid, the second is the progressive adsorption stage where intraparticle diffusion is limiting, and the third region is the final step before equilibrium where intraparticle diffusion begins to slow down because of the low concentration of the solute in the solution. The plots are not linear for the total time interval, which indicates that adsorption is influenced by more than one process. It can be remarked that the plots did not pass by the origin; this was revealing a few degrees of boundary layer control and it further demonstrated that intraparticle diffusion was not the only rate-limiting step, but that other processes could control the adsorption rate. The slope of the linear portion characterizes the rate parameter k_i which corresponds to the intraparticle

diffusion. It was found that the rate constant increases as the initial dye concentration increased.

3.8. Adsorption mechanism

Adsorption mechanism involves the chemical or/and physical adsorption of chemical compounds into substances. Chemical adsorption could be either in terms of chemical bonding or ion exchange; several interactions such as complexation, ion exchange due to surface ionization, and hydrogen bonds may be involved. The different ratio or/and nature of the functional groups for each adsorbent (by means of their strength for electrostatic interactions, e.g., hydrogen bonding) affects tremendously the adsorption capability of the materials [60]. For example, regarding the hydrogen bonding, the strength of a hydrogen bond between an O atom, which is covalently bound to an aliphatic chain is tremendously different from an O atom connected to an aromatic ring. For that reason, different adsorption capacities are observed for different adsorbents and different dyes, due to the different extent and nature of the interactions involved. In order to understand the adsorption mechanism, the point of zero charges (pH$_{PZC}$) of adsorbents, is determined in most research studies. In this manner, a cationic dye (such as MG) adsorption is favored at pH > pHpzc, due to the presence of functional groups such as –OH, –COOH. Subsequently, by controlling the pH value of a wastewater solution, the electrostatic interaction between the adsorbent and the dye may be favored or prevented.

Based on the FTIR spectrum analysis, the mechanism for the adsorption of MG on PLS can be explained. The analysis of FTIR indicates that –OH and –COOH are present on
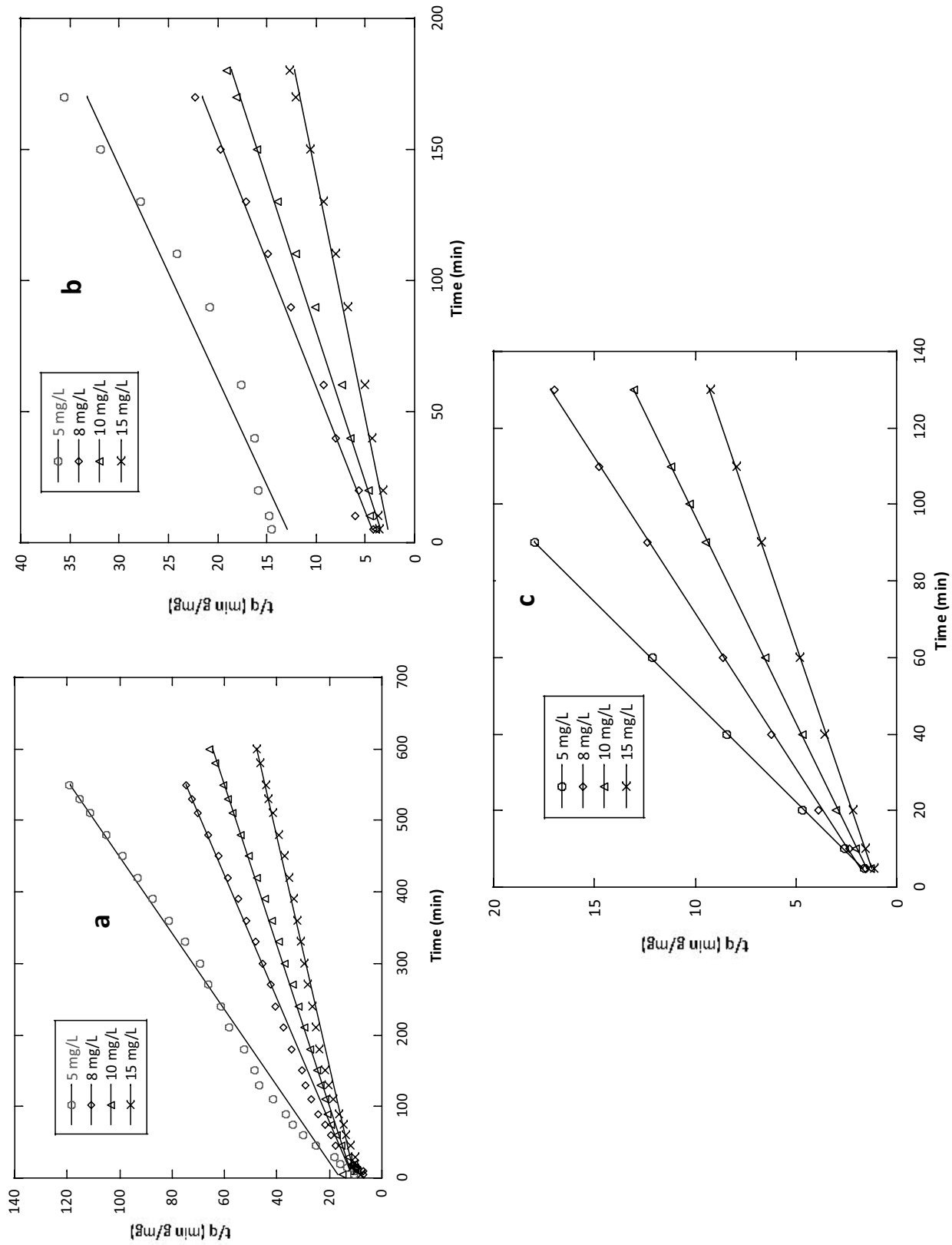
Fig. 13. Pseudo-second-order kinetics for the adsorption of MG by PLS (a) conventional method, (b) sonication, and (c) combined method (conditions: 100 mL of MG solution, initial concentration: 5–15 mg L^{-1}, adsorbent mass: 0.1 g, acoustic power: 69 W, stirring speed: 300 rpm, and temperature: 21°C).
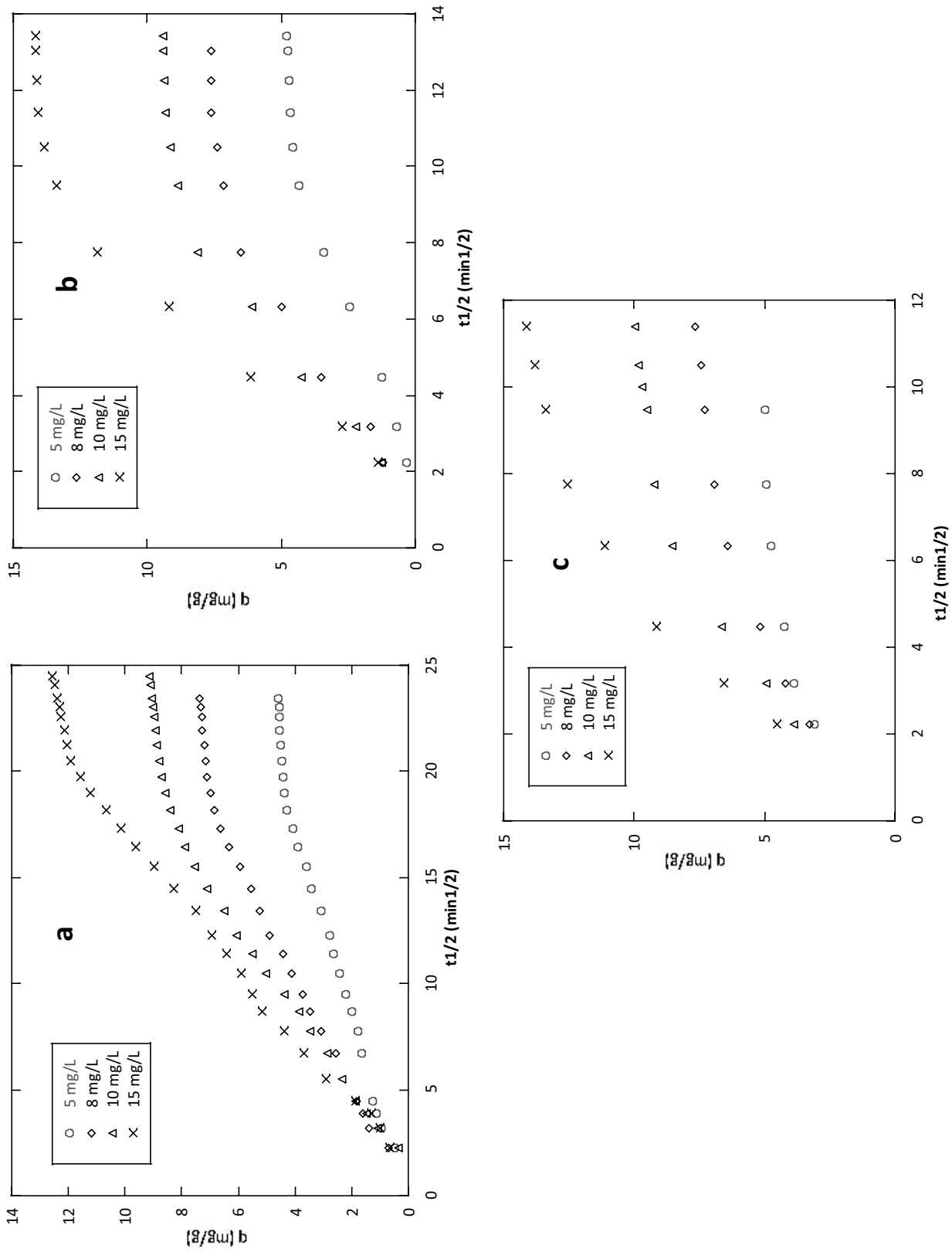
Fig. 14. Intraparticle diffusion plot for the adsorption of MG by PLS: (a) conventional method, (b) sonication, and (c) combined method (conditions: 100 mL of MG solution, initial concentration: 5–15 mg L^{-1}, adsorbent mass: 0.2 g, acoustic power: 69 W, stirring speed: 300 rpm, pH 4, and temperature: 21°C).

PLS surface. In fact, this mechanism could be explained by the electrostatic attraction between hydroxyl and carboxyl groups and the cationic dye molecules. At pH higher than 5.77, the carboxylic groups are deprotonated, and negatively charged carboxylate ligands (COO⁻) bind to the positively charged malachite green molecules [61]. This finding confirms that the adsorption of malachite green by PLS is electrostatic interaction between the negatively charged functional groups and the positively charged dye molecules [62].

4. Conclusion

The present work shows that the PLS can be used as an adsorbent for the removal of malachite green (MG) from aqueous solutions. The quantity of MG adsorbed was found to vary according to the initial dye concentration, the dose of adsorbent, and the pH. The adsorption was considerably enhanced in the presence of the ultrasonic irradiation. The amount of MG adsorption with the assistance of ultrasound was improved with the increase of dye initial concentration, and with the decrease of adsorbent dosage. The coupling of agitation and ultrasound leading to an increasing in the removal of MG. Adsorption isothermal data could be adequately simulated by Langmuir model, followed by the Freundlich and Temkin models. The maximum adsorption capacities calculated by using the Langmuir isotherm were 22.35, 34.45, and 89.72 mg g⁻¹ for the classical method, ultrasound method, and the combined method, respectively. The Adsorption system obeys the pseudo-second-order kinetic model for the combined method (agitation + ultrasound) and it can be predicted by pseudo-first-order kinetic for the classical method. The results of the intra-particle diffusion model proposed that the intraparticle diffusion was not the only step in controlling the rates. The combination of ultrasound and agitation for the adsorption process was proven to be of interest for the treatment of wastewater contaminated with cationic dye like malachite green.

Acknowledgments

References

[1] G. Crini, H.N. Peindy, F. Gimbert, C. Robert, Removal of C.I. Basic Green 4 (Malachite Green) from aqueous solutions by adsorption using cyclodextrin based adsorbent: kinetic and equilibrium studies, Sep. Purif. Technol., 53 (2007) 97–110.
[2] E. Akar, A. Altinisik, Y. Seki, Using of activated carbon produced from spent tea leaves for the removal of malachite green from aqueous solution, Ecol. Eng., 52 (2013) 19–27.
[3] F. Shojaeipoor, B. Masoumi, M.H. Banakar, J. Rastegar, Aminopropyl containing ionic liquid based organosilica as a novel and efficient adsorbent for removal of crystal violet from wastewaters, Chin. J. Chem. Eng., 25 (2017) 1294–1302.
[4] P. Nigam, G. Armour, I.M. Banat, D. Singh, R. Marchant, Physical removal of textile dyes from eluents and solid-state fermentation of dye-adsorbed agricultural residues, Bioresour. Technol., 72 (2000) 219–226.
[5] G.M. Walker, L. Hansen, J.A. Hanna, S.J. Allen, Kinetics of reactive dye adsorption onto dolomitic sorbents, Water Res., 37 (2003) 2081–2089.
[6] Z. Eren, F.N. Acar, Equilibrium and kinetic mechanism for Reactive Black 5 sorption onto high lime Soma fly ash, J. Hazard. Mater., 143 (2007) 226–232.
[7] D. Wu, B. Zhang, C. Li, Z. Zhang, H. Kong, Simultaneous removal of ammonium and phosphate by zeolite synthesized from fly ash as influenced by salt treatment, J. Colloid Interface Sci., 304 (2006) 300–306.
[8] W.T. Tsai, H.R. Chen, Removal of malachite green from aqueous solution using low cost chlorella-based biomass, J. Hazard. Mater., 175 (2010) 844–849.
[9] S.C. Pan, C.C. Lin, D.H. Tseng, Reusing sewage sludge ash as adsorbent for copper removal from wastewater, Resour. Conserv. Recycl., 39 (2003) 79–90.
[10] S. Chowdhury, P. Saha, Sea shell powder as a new adsorbent to remove Basic Green 4 (Malachite Green) from aqueous solutions: equilibrium, kinetic and thermodynamic studies, J. Chem. Eng., 164 (2010) 168–177.
[11] Y.-X. Liu, T.O. Yang, D.X. Yuan, X.Y. Wu, Study of municipal wastewater treatment with oyster shell as biological aerated filter medium, Desalination, 254 (2010) 149–153.
[12] M.E. Haddad, A. Regti, R. Laamari, R. Slimani, R. Mamouni, S.E. Antri, S. Lazar, Calcined mussel shells as a new and eco-friendly biosorbent to remove textile dyes from aqueous solutions, J. Taiwan Inst. Chem. Eng., 45 (2014) 533–540.
[13] M.S. Siboni, A. Khataee, S.W. Joo, Kinetics and equilibrium studies of removal of an azo dye from aqueous solution by adsorption onto scallop, J. Ind. Eng. Chem., 20 (2014) 610–615.
[14] A. Asfaram, M. Ghaedi, K. Dashtian, G.G. Reza, Preparation and characterization of Mn₀.₄Zn₀.₆Fe₂O₄ nanoparticles supported on dead cells of *Yarrowia lipolytica* as a novel and efficient adsorbent/biosorbent composite for the removal of Azo food dyes: central composite design optimization study, ACS Sustainable Chem. Eng., 6 (2018) 4549–4563.
[15] A. Asfaram, M. Ghaedi, M. Hossein, A. Azqhandi, A. Goudarzi, S. Hajati, Ultrasound-assisted binary adsorption of dyes onto 2Mn@CuS/ZnS-NC-AC as a novel adsorbent: application of 3 chemometrics for optimization and modeling, J. Ind. Eng. Chem., 54 (2017) 377–388.
[16] S. Jorfi, R.D.C. Soltani, M. Ahmadi, A. Khataee, M. Safari, Sonoassisted adsorption of a textile dye on milk vetch-derived charcoal supported by silica nanopowder, J. Environ. Manage., 187 (2017) 111–121.
[17] F. Ansari, M. Ghaedi, M. Taghdiri, A. Asfaram, Application of ZnO nanorods loaded on activated carbon for ultrasonic assisted dyes removal: experimental design and derivative spectrophotometry method, Ultrason. Sonochem., 33 (2016) 197–209.
[18] A.R. Bagheri, M. Ghaedi, A. Asfaram, A.A. Bazrafshan, R. Jannesar, Comparative study on ultrasonic assisted adsorption of dyes from single system onto Fe₃O₄ magnetite nanoparticles loaded on activated carbon: experimental design methodology, Ultrason. Sonochem., 34 (2017) 294–304.
[19] D.D. Milenković, A.L. Bojić, V.B. Veljković, Ultrasound-assisted adsorption of 4-dodecylbenzene sulfonate from aqueous solutions by corn cob activated carbon, Ultrason. Sonochem., 20 (2013) 955–962.
[20] R.D.C. Soltani, S. Jorfi, M. Safari, M.-S. Rajaei, Enhanced sonocatalysis of textile wastewater using bentonite-supported ZnO nanoparticles: response surface methodological approach, J. Environ. Manage., 179 (2016) 47–57.
[21] M. Roosta, M. Ghaedi, N. Shokri, A. Daneshfar, R. Sahraei, A. Asghari, Optimization of the combined ultrasonic assisted/adsorption method for the removal of malachite green by gold nanoparticles loaded on activated carbon: experimental design, Spectrochim. Acta, Part A, 118 (2014) 55–65.
[22] O. Hamdaoui, E. Naffrechoux, L. Tifouti, C. Pétrier, Effects of ultrasound on adsorption–desorption of *p*-chlorophenol on granular activated carbon, Ultrason. Sonochem., 10 (2003) 109–114.

[23] O. Hamdaoui, E. Naffrechoux, An investigation of the mechanisms of ultrasonically enhanced desorption, AIChE J., 53 (2007) 363–373.

[24] O. Hamdaoui, E. Naffrechoux, J. Suptil, C. Fachinger, Ultrasonic desorption of *p*-chlorophenol from granular activated carbon, Chem. Eng. J., 106 (2005) 153–161.

[25] O. Hamdaoui, R. Djeribi, E. Naffrechoux, Desorption of metal ions from activated carbon in the presence of ultrasound, Ind. Eng. Chem. Res., 44 (2005) 4737–4744.

[26] O. Hamdaoui, M. Chiha, E. Naffrechoux, Ultrasound-assisted removal of malachite green from aqueous solution by dead pine needles, Ultrason. Sonochem., 15 (2008) 799–807.

[27] O. Hamdaoui, Removal of cadmium from aqueous medium under ultrasound assistance using olive leaves as sorbent, Chem. Eng. Process, 48 (2009) 1157–1166.

[28] O. Hamdaoui, E. Naffrechoux, Adsorption kinetics of 4-chlorophenol onto granular activated carbon in the presence of high frequency ultrasound, Ultrason. Sonochem., 16 (2009) 15–22.

[29] L. Nouri, O. Hamdaoui, Ultrasonication-assisted sorption of cadmium from aqueous phase by wheat bran, J. Phys. Chem. A, 111 (2007) 8456–8463.

[30] L.H. Thompson, L.K. Doraiswamy, Sonochemistry: science and engineering, Ind. Eng. Chem. Res., 38 (1999) 1215–1249.

[31] Y.G. Adewuyi, Sonochemistry: environmental science and engineering applications, Ind. Eng. Chem. Res., 40 (2001) 4681–4715.

[32] B. Abussaud, H.A. Asmaly, T.A. Ihsanullah, V.K. Saleh, T. Gupta, M.A. Atiehlaoui, Sorption of phenol from waters on activated carbon impregnated with iron oxide, aluminum oxide and titanium oxide, J. Mol. Liq., 213 (2016) 351–359.

[33] S. Sun, S. Wang, P. Wang, Q. Wu, S. Fang, Ultrasound assisted morphological control of mesoporous silica with improved lysozyme adsorption, Ultrason. Sonochem., 23 (2015) 21–25.

[34] N. Pazos-Perez, J. Schäferhans, E.V. Skorb, A. Fery, D.V. Andreeva, Ultrasound driven formation of metal-supported nanocatalysts, Microporous Mesoporous Mater., 154 (2012) 164–169.

[35] M.J. Temkin, V. Pyzhev, Recent modifications to Langmuir Isotherms, Acta Physiochim. USSR, 12 (1940) 217–222.

[36] Y.S. Ho, D.A. John Wase, C.F. Forster, Batch nickel removal from aqueous solution by sphagnum moss peat, Water Res., 29 (1995) 1327–1332.

[37] S.S. Tahir, N. Rauf, Removal of a cationic dye from aqueous solutions by adsorption onto bentonite clay, Chemosphere, 63 (2006) 1842–1848.

[38] J. Zhang, Y. Li, Adsorption of malachite green from aqueous solution onto carbon prepared from *Arundo donax* root, J. Hazard. Mater., 150 (2008) 774–778.

[39] B.H. Hameed, M.I. El-Khaiary, Malachite green adsorption by rattan sawdust: isotherm, kinetic and mechanism modeling, J. Hazard. Mater., 159 (2008) 574–579.

[40] S.D. Khattri, M.K. Singh, Removal of malachite green from dye wastewater using neem sawdust by adsorption, J. Hazard. Mater., 167 (2009) 1089–1094.

[41] M.-H. Baek, C.O. Ijagbemi, S.-J. O, D.-S. Kim, Removal of malachite green from aqueous solution using degreased coffee bean, J. Hazard. Mater., 176 (2010) 820–828.

[42] H. Zhang, Y. Tang, X. Liu, K. Zhigang, X. Su, D. Cai, X. Wang, Y. Liu, Q. Huang, Z. Yu, Improved adsorptive capacity of pine wood decayed by fungi *Poria cocos* for removal of malachite green from aqueous solutions, Desalination, 274 (2011) 97–104.

[43] A.S. Sartape, A.M. Mandhare, V.V. Jadhav, P.D. Raut, M.A. Anuse, S.S. Kolekar, Removal of malachite green dye from aqueous solution with adsorption technique using *Limonia acidissima* (wood apple) shell as low cost adsorbent, Arabian J. Chem., 10 (2017) S3229–S3238.

[44] S. Banerjee, G.C. Sharma, R.K. Gautam, M.C. Chattopadhyaya, S.N. Upadhyay, Y.C. Sharma, Removal of Malachite Green, a hazardous dye from aqueous solutions using *Avena sativa* (oat) hull as a potential adsorbent, J. Mol. Liq., 213 (2016) 162–172.

[45] S.Y. Kazemia, P. Biparvaa, E. Ashtiani, *Cerastoderma lamarcki* shell as a natural, low cost and new adsorbent to removal of dye pollutant from aqueous solutions: equilibrium and kinetic studies, J. Ecol. Eng., 88 (2016) 82–89.

[46] S. Wang, E. Ariyanto, Competitive adsorption of malachite green and Pb ions on natural zeolite, J. Colloid Interface Sci., 314 (2007) 25–31.

[47] P. Janos, Sorption of basic dyes onto iron humate, Environ. Sci. Technol., 37 (2003) 5792–5798.

[48] T.K. Arumugama, P. Krishnamoorthy, N.R. Rajagopalan, S. Nanthini, D. Vasudevan, Removal of malachite green from aqueous solutions using a modified chitosan composite, Int. J. Biol. Macromol., 128 (2019) 655–664.

[49] N. Gupta, A.K. Kushwaha, M.C. Chattopadhyaya, Application of potato (*Solanum tuberosum*) plant wastes for the removal of methylene blue and malachite green dye from aqueous solution, Arabian J. Chem., 9 (2016) S707–S716.

[50] S. Arivoli, M. Hema, P. Martin, D. Prasath, Adsorption of malachite green onto carbon prepared from borassus bark, Arabian J. Sci. Eng., 34 (2009) 31–42.

[51] S. Parthasarathy, N. Manju, M. Hema, S. Arivoli, Removal of malachite green from industrial waste-water by activated carbon prepared from cashew nut bark Alfa Universal, Int. J. Chem., 2 (2011) 41–51.

[52] C.P. Sekhar, S. Kalidhasan, V. Rajesh, N. Rajesh, Biopolymer adsorbent for the removal of malachite green from aqueous solution, Chemosphere, 77 (2009) 842–847.

[53] S. Chowdhury, R. Mishra, P. Saha, P. Kushwaha, Adsorption thermodynamics, kinetics and isosteric heat of adsorption of malachite green onto chemically modified rice husk, Desalination, 265 (2011) 159–168.

[54] P. Saha, S. Chowdhury, S. Gupta, I. Kumar, R. Kumar, Assessment on the removal of malachite green using tamarind fruit shell as biosorbent, Clean Soil Air Water, 38 (2010) 437–445.

[55] S. Lagergren, About the theory of so-called adsorption of soluble substances, Kuling. Sven. Vetenskapsakad. Handl., 24 (1898) 1–39.

[56] Y.S. Ho, G. McKay, Sorption of dye from aqueous solution by peat, Chem. Eng. J., 70 (1998) 115–124.

[57] Y.S. Ho, G. McKay, The kinetics of sorption of divalent metal ions onto sphagnum moss peat, Water Res., 34 (2000) 735–742.

[58] M.A. Hubbe, S. Azizian, S. Douven, Implications of apparent pseudo-second-order adsorption kinetics onto cellulosic materials: a review, BioResources, 14 (2019) 7582–7626.

[59] W.J. Weber, J.C. Morris, Kinetics of adsorption on carbon from solution, J. Sanitary Eng. Div., 89 (1963) 31–59.

[60] K.A. Adegoke, O.S. Bello, Dye sequestration using agricultural wastes as adsorbents, Water Resour. Ind., 12 (2015) 8–24.

[61] C.-H. Wu, Adsorption of reactive dye onto carbon nanotubes: equilibrium, kinetics and thermodynamics, J. Hazard. Mater., 144 (2007) 93–100.

[62] A. Saeed, M. Sharif, M. Iqbal, Application potential of grapefruit peel as dye sorbent: kinetics, equilibrium and mechanism of crystal violet adsorption, J. Hazard. Mater., 179 (2010) 564–572.